

Looking for hints of a reconstructible seesaw model at the Large Hadron Collider

Gulab Bambhaniya,^{1,*} Srubabati Goswami,^{1,†} Subrata
Khan,^{1,‡} Partha Konar,^{1,§} and Tanmoy Mondal^{1,2,¶}

¹*Physical Research Laboratory (PRL), Ahmedabad-380009, Gujarat, India*

²*Indian Institute of Technology, Gandhinagar, India.*

(Dated: April 13, 2015)

Abstract

We study the production of heavy neutrinos at the Large Hadron Collider (LHC) through the dominant s-channel production mode as well as the vector boson fusion (VBF) process. We consider the TeV scale minimal linear seesaw model containing two heavy singlets with opposite lepton number. This model is fully reconstructible from oscillation data apart from an overall normalization constant which can be constrained from meta-stability of the electroweak vacuum and bounds coming from lepton flavor violation (LFV) searches. Dirac nature of heavy neutrinos in this model implies suppression of the conventional same-sign-dilepton signal at the LHC. We analyze the collider signatures with tri-lepton final state and missing transverse energy as well as VBF type signals which are characterized by two additional forward tagged jets. Our investigation reveals that due to stringent constraints on light-heavy mixing coming from LFV and meta-stability bounds, the model can be explored only for light to moderate mass range of heavy neutrinos. We also note that in case of a positive signal, flavor counting of the final tri-lepton channel can give information about the mass hierarchy of the light neutrinos.

PACS numbers: 12.60.-i, 14.60.St, 13.35.Hb, 13.85.Qk

Keywords: Beyond Standard Model, Heavy Neutrinos, Hadronic Colliders, Lepton production

*Electronic address: gulab@prl.res.in

†Electronic address: sruba@prl.res.in

‡Electronic address: subrata@prl.res.in

§Electronic address: konar@prl.res.in

¶Electronic address: tanmoym@prl.res.in

1. INTRODUCTION

The discovery of the Higgs boson at the Large Hadron Collider both by ATLAS [1] and CMS [2] collaborations have put the Standard Model (SM) on a firm footing. However, no signal of physics beyond the Standard Model (BSM) has been found so far at the LHC. On the other hand, convincing indications of BSM physics have already emerged from the phenomenon of neutrino oscillation observed in terrestrial experiments. These results have conclusively established that neutrinos have non-zero mass and flavor mixing. Oscillation data together with the cosmological bound on sum of neutrino masses ($\Sigma m_i < 0.23$ eV including the PLANCK data [3]) indicate that neutrino masses are much smaller as compared to the other fermions in the SM. Such small masses can be generated naturally by the seesaw mechanism. The origin of seesaw is the dimension 5 effective operator $\frac{c_5}{M}LLHH$, where $L(H)$ being the SM lepton(Higgs) doublet and c_5 is a dimensionless coupling, M is the mass scale at which the effective operator gets generated [4]. Such operators arise by integrating out heavy fields added to the SM Lagrangian and they violate lepton number by two units. The smallness of neutrino mass in these models is related to the scale of lepton number violation which is required to be very high $\sim \mathcal{O}(10^{15}$ GeV) to generate neutrino masses in the right ballpark. The most economical in terms of particle contents is the type-I seesaw in which heavy singlet right-handed neutrinos are added to the SM Lagrangian [5–9]. However, the natural seesaw scale is far beyond the reach of the LHC. To have signatures of seesaw models at the LHC, the heavy neutrino (N) mass needs to be $\sim \mathcal{O}$ (TeV). However, if one lowers the scale of seesaw to TeV then it also requires much smaller neutrino Yukawa couplings ($\sim 10^{-6}$) to obtain correct light neutrino masses. Such small Yukawa couplings lead to suppression of the production of the heavy neutrinos in natural TeV scale Type-I seesaw models. This leads to the question whether it is possible to achieve both the requirements simultaneously, i.e. having TeV scale heavy neutrinos along with large Yukawa coupling leading to large light-heavy mixing. Such possibilities can be realized in some specific mass textures [10–18]. Other options include models with higher-dimensional operators arising due to exchange of new particles belonging to larger representations [19–27], radiative mass generations [28–35] etc. One of the most popular options to generate TeV scale seesaw is through the inverse seesaw models in which one includes additional singlet states. These models were first proposed in the context of E(6) Grand Unified Theories [36]. In these models the seesaw scale is decoupled from the scale of lepton number violation and the smallness of neutrino mass originates from the small lepton number violating terms in the Lagrangian.

In type-I Seesaw model the heavy and light neutrinos are both Majorana particles. It is well

known that Majorana nature of neutrinos can be established by observing a positive signal in neutrino-less double beta decay experiments. It was noticed in [37], in the context of the Left-Right symmetric model that resonant production of N and its subsequent decay giving same-sign di-lepton (SSDL) signal in colliders can also constitute evidence for Majorana nature of neutrinos. Given the importance of this signal, there have been several studies of this channel at the hadron colliders [38–43] including searches at the LHC [44]. Enhanced contribution from infrared t-channel, especially for heavier masses was proposed [45, 46] together with s-channel production.

The heavy neutrinos in inverse seesaw model are of pseudo-Dirac nature and in this case the SSDL signal is suppressed by the small lepton number violating coupling. For such models the heavy neutrinos are produced by the s-channel process along with a charged lepton. This neutrino further decays to a second lepton (of sign opposite to the first lepton to conserve lepton number) together with a W-boson. The W-boson can further decay leptonically to produce a lepton and a neutrino. Thus the final signal consists of tri-lepton and missing energy which is expected to have tiny contamination from standard model backgrounds. Detailed studies including the SM background in the context of pseudo-Dirac neutrinos have been done in [42, 47]. Similar studies in the context of Left-Right symmetric model, non-minimal supersymmetric inverse seesaw models and Type-III seesaw model have been performed in [48], [49] and [50] respectively. Experimental searches for multi-lepton signals have been carried out by the CMS collaboration using an integrated luminosity of 19.5 fb^{-1} with center of mass energy $\sqrt{s} = 8 \text{ TeV}$ at the LHC [51]. They considered at least three leptons in the final state using a search strategy not specific to any particular model.

In this work, we consider the minimal linear seesaw model (MLSM) studied in [52, 53] as an example of the TeV scale seesaw model. This is a variant of the inverse seesaw model but in this case the minimal scheme consists of adding just two heavy singlets with opposite lepton number as opposed to four heavy neutrinos in canonical minimal inverse seesaw models [54]. It was shown in [52] that the Yukawa couplings matrices for this model can be fully reconstructed in terms of the oscillation parameters apart from an overall normalization factor. It was further shown in [53] that this normalization constant can be constrained from consideration of the meta-stability of the electroweak vacuum and lepton flavor violation bounds. The heavy neutrinos in this model are of Dirac type and the SSDL signal is suppressed¹. In the context of this model we consider two possible production channels for the heavy neutrinos resulting in two different classes of signals. The first one of this is the s-channel process to produce heavy Dirac neutrinos associated with a lepton and

¹ Due to same reason heavy neutrino contribution towards $0\nu\beta\beta$ is suppressed [53].

finally giving the tri-lepton and missing energy signal. The second one is the production of heavy neutrinos through vector boson fusion (VBF) in which two electroweak vector bosons coming from two partons ‘fuse’ to produce the signal under consideration (tri-leptons) along with two highly forward jets. It becomes important in the context of hadron colliders since the tagging of forward jets allows us to reduce the background considerably. Also the lack of color exchange between these jets makes the central region free from the color activities and this is exploited by vetoing central jets; see [55] and references therein in the context of Higgs search. This helps in minimizing the backgrounds further. For these reasons VBF remains an important channel to look for new physics [56–58] at hadron colliders.

We consider both normal hierarchy (NH) as well as inverted hierarchy (IH) for the light neutrino mass spectra. We also estimate the corresponding standard model backgrounds for the 14 TeV LHC. In each case, we perform a realistic simulation with extensive event selections using **MadGraph** and **PYTHIA**.

The paper is organized as follows: Sec. 2 contains a brief description of the model. The production and decay of the right handed neutrino at LHC, are discussed in Sec. 3. Simulation details and results are presented in Sec. 4, while in Sec. 5 we discuss discovery potential of the signals at the LHC. Finally, we conclude in Sec. 6.

2. THE LINEAR SEESAW MODEL

The most general Lagrangian containing heavy singlet fields N_R and S with opposite lepton numbers, is given by

$$-\mathcal{L} = \overline{N}_R Y_\nu \tilde{\phi}^\dagger l_L + \overline{S} Y_S \tilde{\phi}^\dagger l_L + \overline{S} M_N N_R^c + \frac{1}{2} \overline{S} \mu S^c + \frac{1}{2} \overline{N}_{R\mu N} N_R^c + \text{h.c.}, \quad (1)$$

where $l_L = (\nu_x, x)_L^T$, $x = e, \mu, \tau$.

Once the symmetry is broken spontaneously, the Higgs field ϕ obtains a vacuum expectation value (VEV) equal to $v/\sqrt{2}$. This generates the Dirac mass term $m_D = Y_\nu v/\sqrt{2}$ and the lepton number breaking mass term $m_S = Y_S v/\sqrt{2}$. In the linear seesaw models [59–61] one assumes m_S to be small and non-zero while the μ and the μ_N terms are set to zero. This can be done since they contribute towards light neutrino mass in the sub-leading orders [62]. Since lepton number violating mass terms are set to zero, the heavy neutrinos are purely Dirac type. Then the mass

matrix takes the form

$$\mathcal{M}_\nu = \begin{pmatrix} 0 & m_D^T & m_S^T \\ m_D & 0 & M_N \\ m_S & M_N^T & 0 \end{pmatrix}, \quad (2)$$

in the (ν_L, N_R^c, S^c) basis.

The minimal model which can successfully generate two light neutrinos with non-zero mass is when only two extra heavy singlets are added to the SM Lagrangian. This is called the Minimal Linear Seesaw Model (MLSM) [52, 53]. The full mass matrix has dimension 5×5 and can be written as ,

$$\mathcal{M}_\nu = \begin{pmatrix} 0 & m_D'^T \\ m_D' & M \end{pmatrix}, \quad (3)$$

where $m_D'^T = (m_D^T, m_S^T)$ and

$$M = \begin{pmatrix} 0 & M_N \\ M_N & 0 \end{pmatrix}. \quad (4)$$

For the minimal case M_N is just a number, not a matrix. \mathcal{M}_ν can be diagonalized by a 5×5 unitary matrix U_0 as

$$U_0^T \mathcal{M}_\nu U_0 = \mathcal{M}_\nu^{\text{diag}}, \quad (5)$$

where $\mathcal{M}_\nu^{\text{diag}} = \text{diag}(m_1, m_2, m_3, M_1, M_2)$. Following a two-step diagonalization procedure [63], U_0 can be expressed as,

$$U_0 = \begin{pmatrix} (1 - \frac{1}{2}\epsilon) U_\nu & m_D^\dagger (M^{-1})^* U_R \\ -M^{-1} m_D U_\nu & (1 - \frac{1}{2}\epsilon') U_R \end{pmatrix} \equiv \begin{pmatrix} U_L & V \\ S & U_H \end{pmatrix}, \quad (6)$$

where, U_L is the U_{PMNS} mixing matrix, and V, S are the light-heavy mixing matrices. Interaction of heavy neutrinos with the SM fields are determined by the mixing matrix V , whose elements will be denoted as V_{lN} hereafter. We would notice afterwards that the strong constraints on some elements of this matrix *i.e.* V_{eN} and $V_{\mu N}$ would restrict the production signal. The diagonalizing matrix is now non-unitary which is characterized by the factor $(1 - \epsilon/2)$. The non-unitary corrections ϵ and ϵ' are given in [63, 64]. U_ν is the unitary component of U_{PMNS} which is same as U_{PMNS} for $\epsilon \ll 1$. We use the standard parametrization for this:

$$U_\nu = \begin{pmatrix} c_{12} c_{13} & s_{12} c_{13} & s_{13} e^{-i\delta} \\ -c_{23} s_{12} - s_{23} s_{13} c_{12} e^{i\delta} & c_{23} c_{12} - s_{23} s_{13} s_{12} e^{i\delta} & s_{23} c_{13} \\ s_{23} s_{12} - c_{23} s_{13} c_{12} e^{i\delta} & -s_{23} c_{12} - c_{23} s_{13} s_{12} e^{i\delta} & c_{23} c_{13} \end{pmatrix} P, \quad (7)$$

where $c_{ij} = \cos \theta_{ij}$, $s_{ij} = \sin \theta_{ij}$ and δ denotes the Dirac CP phase. The Majorana phase matrix P is expressed as $P = \text{diag}(e^{-i\alpha}, e^{i\alpha}, 1)$, there is only one Majorana phase because one of the mass eigenvalues is zero. In table I, we have presented the 3σ allowed range of oscillation parameters. Note that the phases are completely unconstrained at present.

Using the seesaw approximation one obtains the light neutrino mass matrix,

$$m_{\text{light}} = m_D'^T M^{-1} m_D'. \quad (8)$$

This being a rank 2 matrix the light neutrinos belonging to this model are hierarchical. Thus there are two possible mass spectra:

- ◊ Normal Hierarchy (NH): $(m_1 < m_2 < m_3)$
- ◊ Inverted Hierarchy (IH): $(m_3 \ll m_2 \approx m_1)$.

In MLSM, Y_ν and Y_S are 3×1 matrices (cf. Eq. 1) and can be considered as two independent vectors

$$Y_\nu \equiv y_\nu \hat{\mathbf{a}}; \quad Y_S \equiv y_s \hat{\mathbf{b}}, \quad (9)$$

where $\hat{\mathbf{a}}$ and $\hat{\mathbf{b}}$ denotes complex vectors with unit norm while y_ν and y_s represent the norms of the Yukawa matrices Y_ν and Y_S , respectively. Using Eq. 8 and 9 one can reconstruct the Yukawa matrices Y_ν and Y_S in terms of the oscillation parameters barring an overall normalization factor. The parametrization of the Yukawa matrices depend on the mass hierarchy and can be expressed as [52, 53],

$$\begin{aligned} Y_\nu &= \frac{y_\nu}{\sqrt{2}} \left(\sqrt{1+\rho} U_j^\dagger + e^{i\frac{\pi}{2}} \sqrt{1-\rho} U_k^\dagger \right), \\ Y_S &= \frac{y_s}{\sqrt{2}} \left(\sqrt{1+\rho} U_j^\dagger - e^{i\frac{\pi}{2}} \sqrt{1-\rho} U_k^\dagger \right), \end{aligned} \quad (10)$$

where, $j = 2, k = 3$ for NH and $j = 2, k = 1$ for IH. U_j 's denote the columns of the unitary matrix U_ν that diagonalizes the light neutrino mass matrix m_{light} in Eq. 8. The parameter ρ is given as,

$$\rho = \frac{\sqrt{1+r} - \sqrt{r}}{\sqrt{1+r} + \sqrt{r}} \quad (NH), \quad \rho = \frac{\sqrt{1+r} - 1}{\sqrt{1+r} + 1} \quad (IH). \quad (11)$$

Here r denotes the ratio of the solar and atmospheric mass squared differences, $r = \Delta m_\odot^2 / \Delta m_{\text{atm}}^2$, with $\Delta m_\odot^2 \equiv m_2^2 - m_1^2$ and $\Delta m_{\text{atm}}^2 \simeq m_3^2 - m_1^2$ ($m_2^2 - m_3^2$) for NH (IH).

The overall coupling y_ν can be constrained from the metastability of the electro-weak vacuum and LFV [53]. For NH the most stringent constraint comes from LFV, whereas for IH case vacuum

meta-stability constraint is more restrictive. This is because of cancellations occurring for IH for LFV processes [53]. The dependence of the bound on y_ν from meta-stability and LFV on the heavy neutrino mass has been shown in [53]. The metastability bound on y_ν varies approximately in the range 0.4 - 0.5 for M_N varying in the range 100 - 1000 GeV. This bound is independent of the oscillation parameters. However, significant variation on the bound on y_ν from LFV constraint is possible within the allowed range of oscillation parameters, mostly due to unconstrained phases, δ and α . Details of these dependence can be followed from Fig. 1. For a particular M_N , the strength of the signal at LHC would depend on the value of y_ν . To maximise the signal we therefore choose the value of y_ν at the peak for NH case. However, for IH case the peak value is much above the vacuum metastability bound and therefore we choose maximum allowed value of y_ν satisfying the metastability bound. The corresponding parameter values are depicted in table I for NH (case I) and IH. Note that, the above mentioned cancellations within the terms, ensure the peak position corresponds to $\alpha + \delta = 3\pi/2(3\pi/4)$ for NH (IH), which is also evident in Fig. 1. We have chosen $\delta = 0$ in our analysis. For some other values of δ , the phase α has to be chosen so that one is at the peak. In Fig. 1 we also show the variation of this bound with respect to the θ_{23} mixing angle in lower octant (LO, $\theta_{23} < \pi/4$) and higher octant (HO, $\theta_{23} > \pi/4$). The y_ν value 0.4(0.075) corresponds to IH(NH: Case-I) scenario for $M_N = 100$ GeV, which we will use in our analysis. These will be translated into the bounds on the mixing matrix elements, V_{lN} , depending on the heavy neutrino mass M_N . Since y_s is extremely small ($\mathcal{O}(10^{-10})$), Y_S does not play any role in determining V_{lN} . The elements of the matrix V (or V_{lN}) can be expressed in terms of U_{PMNS} matrix, ρ and y_ν as follows:

$$\begin{aligned}
V_{eN_1} &= \frac{-i}{\sqrt{2}M_N} \frac{y_\nu v}{2} \left[\sqrt{1+\rho} (U_{PMNS})_{12}^* + i \sqrt{1-\rho} (U_{PMNS})_{11}^* \right] \\
&\simeq \frac{y_\nu v}{4M_N} \left[e^{i(\alpha+\delta)} (-2 + \sqrt{r}) r^{\frac{1}{4}} s_{12} - 2i s_{13} \right] + \mathcal{O}((\sqrt{r}, s_{13})^2) \\
V_{\mu N_1} &= \frac{-i}{\sqrt{2}M_N} \frac{y_\nu v}{2} \left(\sqrt{1+\rho} (U_{PMNS})_{22}^* + i \sqrt{1-\rho} (U_{PMNS})_{21}^* \right) \\
&\simeq \frac{y_\nu v}{4M_N} \left[(-2 + \sqrt{r}) (e^{i\alpha} r^{\frac{1}{4}} c_{12} c_{23} + i s_{23}) + 2 e^{i(\alpha+\delta)} r^{\frac{1}{4}} s_{12} s_{23} s_{13} \right] + \mathcal{O}((\sqrt{r}, s_{13})^2). \quad (12)
\end{aligned}$$

The above expressions are for NH scenario and similar expressions can be computed for IH also. The element V_{eN_2} ($V_{\mu N_2}$) differs from V_{eN_1} ($V_{\mu N_1}$) by a phase factor. Note that in Table I, we also consider a second set of oscillation parameters for NH (NH: Case II) corresponding to a lower value of y_ν of 0.056 with θ_{23} in the higher octant. This value is chosen such that $V_{\mu N}$ is maximum and muon signal may be larger, since muon has higher efficiency for detection.

To get some perspective on the degree of suppression in cross section coming from these con-

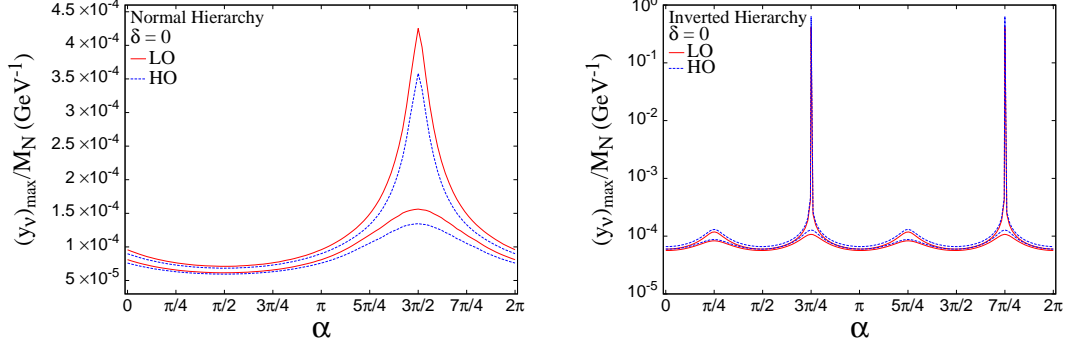


FIG. 1: Bound on y_ν/M_N as a function of Majorana phase α , varying the oscillation parameters in the allowed 3σ range. Red-solid(Blue-dashed) curve corresponds to atmospheric angle (θ_{23}) residing in LO(HO) region. (Left plot) The plot is for NH scenario, where highest allowed value of y_ν/M_N lies in LO region. (Right plot) The same plot for IH scenario.

Parameter Bound	$\Delta_\odot^2 [10^{-5} \text{ eV}^2]$	$\Delta_{\text{atm}}^2 [10^{-3} \text{ eV}^2]$	$\sin^2 \theta_{12}$	$\sin^2 \theta_{23}$	$\sin^2 \theta_{13}$	δ
3σ range (NH)	7.12 – 8.20	2.31 – 2.74	0.27 – 0.37	0.36 – 0.68	0.017 – 0.033	$0 - 2\pi$
(IH)		2.21 – 2.64		0.37 – 0.67		
Used value (NH: Case - I)	7.15	2.73	0.27	0.36	0.033	0.0
Used value (NH: Case - II)	7.13	2.73	0.27	0.68	0.033	0.0
Used value (IH)	7.25	2.40	0.34	0.57	0.021	0.0

TABLE I: Allowed 3σ ranges of oscillation parameters and benchmark values of these parameters used in our analysis to get the signal allowed by LFV and vacuum metastability. Case-I corresponds to the peak in Fig. 1(Left panel), while Case-II corresponds to a lower value of y_ν/M_N , for which $V_{\mu N}$ is maximum. Value of Majorana phase α is set at $3\pi/2$ ($3\pi/4$) for NH(IH) scenario.

straints we note down the corresponding V_{lN} values for $M_N = 100 \text{ GeV}$ as: $V_{eN} = 1.95 \times 10^{-3}$, $V_{\mu N} = 2.93 \times 10^{-2}$ and $V_{\tau N} = 8.83 \times 10^{-2}$ for NH (Case-I) scenario, whereas, $V_{eN} = 1.43 \times 10^{-3}$, $V_{\mu N} = 4.14 \times 10^{-2}$ and $V_{\tau N} = 5.48 \times 10^{-2}$ for NH (Case-II) respectively. For IH these values are $V_{eN} = 0.48$, $V_{\mu N} = 4.15 \times 10^{-9}$ and $V_{\tau N} = 0.109$. Note that since our model is fully reconstructible and the only unknown parameter is y_ν which can be constrained from LFV and meta-stability bounds, we have definite predictions for the parameters V_{lN} and these values are different for NH and IH scenarios. Bounds on V_{lN} can also come from Electroweak Precision Data (EWPD) [65]. Our bounds for NH are consistent with these bounds. For IH we get a larger value for V_{eN} . However it is to be noted that the EWPD bounds are obtained assuming mixing with a single charged lepton and can be evaded in presence of cancellations or mixing with the other charged leptons

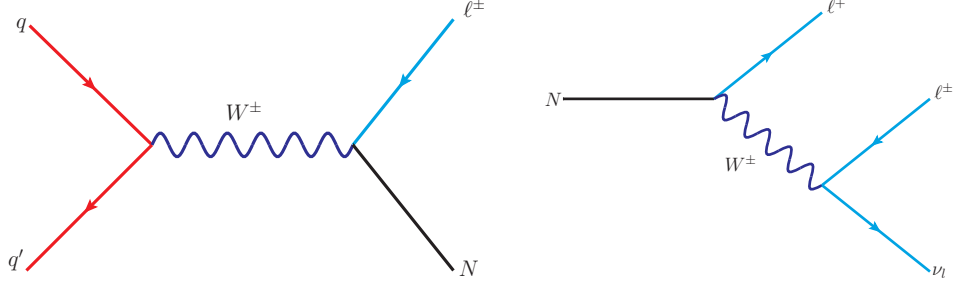


FIG. 2: (Left plot) Leading order s-channel diagram for heavy neutrino production at hadron colliders, and (Right plot) representative diagram for one of the decay mode of the heavy neutrino. These two figures lead to tri-lepton + \cancel{E}_T signal considered in the analysis.

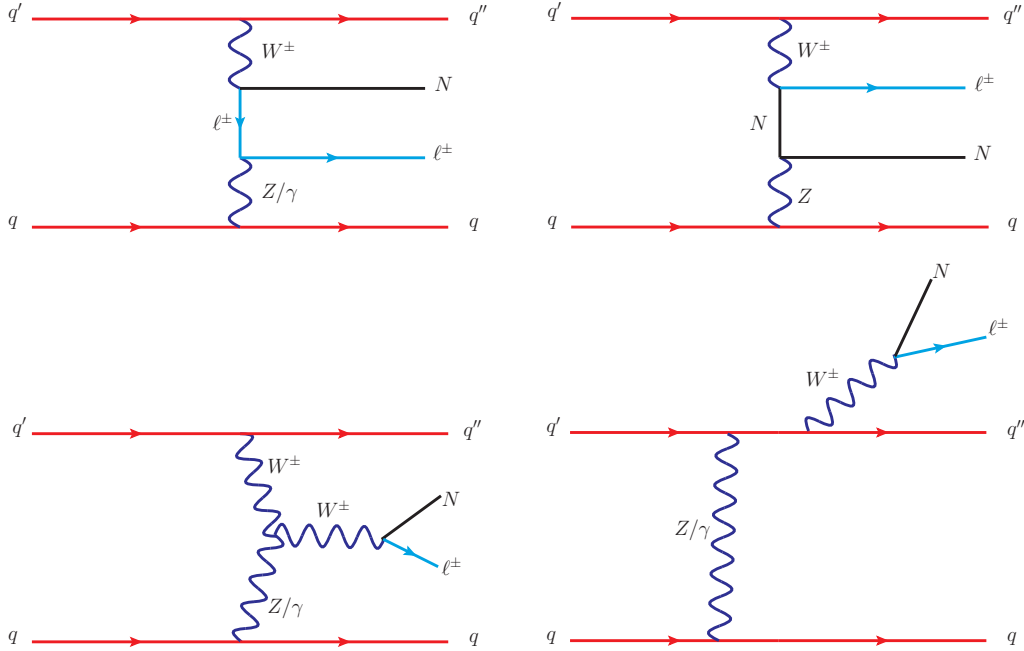


FIG. 3: Representative parton level diagrams contributing to $N\ell jj$ production through vector boson fusion at hadron colliders. Mirror diagrams are not shown here and also the last diagram is one of the four diagrams with W^\pm emitting from each of the quark legs.

[42].

3. PHENOMENOLOGY AT THE LHC

The dominant production channel of the heavy neutrinos at LHC is the s-channel process through virtual W-boson exchange. At the leading order the parton level process ($q\bar{q}' \rightarrow W^\pm \rightarrow \ell^\pm N$) is depicted in Fig. 2(left plot). The heavy neutrinos can also be produced through the

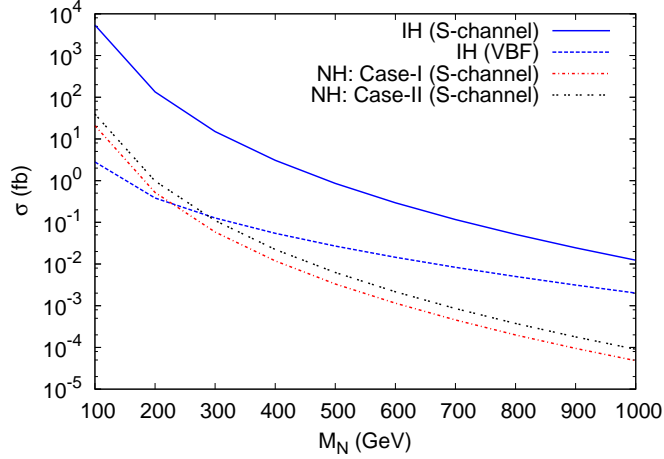


FIG. 4: The total cross section is shown for production of heavy neutrino associated with light lepton ($pp \rightarrow N\ell$, where $\ell = e, \mu$) at the 14 TeV LHC through the leading order s-channel process, while dotted lines represent VBF production cross section.

VBF process where production of N is associated with two forward jets. Fig. 3 contains the representative parton level Feynman diagrams for VBF processes². Estimated total production cross sections of these heavy Dirac neutrinos at the 14 TeV LHC in IH scenario are shown in Fig. 4 for both s -channel (solid-line) as well as VBF (dashed-line). For NH scenario the s -channel production cross sections are shown in the same figure for two different cases (*c.f.* Table I), Case-I (Red dot-dashed line) and Case-II (Black double dotted line). Basic cuts such as $p_{T\ell} > 20$ GeV and $|\eta_\ell| < 2.5$ are applied and y_ν values mentioned in the previous section are used. It is seen from the figure that although case II corresponds to a lower value of y_ν since $V_{\mu N}$ is larger, the production cross-section is slightly larger. Since the VBF cross-section is much lower we do not present the VBF cross-section for the NH case. In these analyses CTEQ6L1 [68] parton distribution functions have been used with the factorization scale set at the heavy neutrino mass M_N .

Heavy neutrinos N can decay into charged lepton or neutrino associated with gauge (or Higgs) boson.

$$N \rightarrow W^\pm l^\mp / Z \nu_l / H \nu_l, \quad \text{where } l \equiv e, \mu, \tau. \quad (13)$$

A representative diagram for decay of N ($N \rightarrow \ell^\mp W^\pm$) is shown in Fig. 2(right plot).

In Fig. 5 we present the branching ratios for these decay channels as a function of heavy neutrino mass M_N both in the case of normal hierarchy (left) and inverted hierarchy (right). Total decay

² Note that there are some diagrams which are not truly VBF type, i.e. two gauge bosons are not fused via t-channel (e.g. bottom right diagram in Fig. 3), but they can lead to the same final states. These diagrams are necessary for the requirements of gauge invariance and included both for BG [66, 67] and signal calculations.

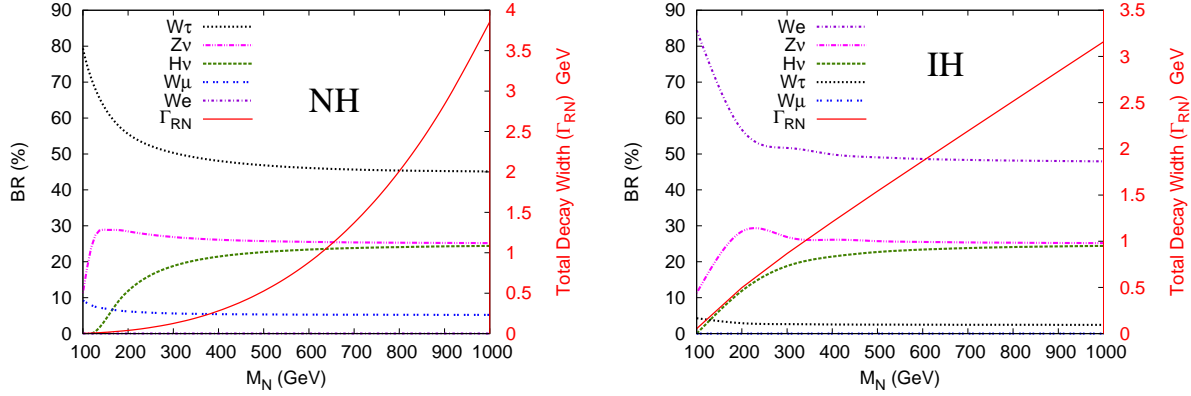


FIG. 5: The decay branching ratios of the heavy neutrino (N) in different channels as a function of its mass in the case of normal hierarchy, Case-I, (left) and inverted hierarchy (right). Total decay widths in each case are also demonstrated with the solid line in the same figure.

widths in each case are also demonstrated with the solid line in each figure. Identifying that the charged lepton decay modes for heavy neutrino i.e. $N \rightarrow W^\pm l^\mp$ being the main channel for search at the hadron collider, we discuss the corresponding decay modes in detail for both scenarios. The figure clearly shows that for NH, Case-I³, heavy neutrinos mostly decay into tau lepton (τ) and W boson. On the other hand for IH, decay into the first generation lepton (e) possesses the maximum branching ratio. For NH the decay to μ is low and decay to e is severely suppressed, while for IH, the decay to τ has a lower ratio and decay to μ is negligible. The W^\pm can have hadronic decay modes ($W^\pm \rightarrow jj$) or leptonic decay modes ($W^\pm \rightarrow l^\pm \nu$). The tri-lepton signal $pp \rightarrow l^\pm l^\mp l^\pm \nu$ comes from the later decay mode⁴.

Other than charged lepton decay mode, N can also decay to Z -boson or Higgs boson associated with neutrinos as listed in Eq. 13. The corresponding branching ratios are also shown in Fig. 5. Note that the branching ratio for $Z\nu$ is suppressed for lower values of the masses of the heavy neutrinos essentially because of W mass threshold. For the $H\nu$ decay mode, the Higgs mass threshold suppresses the decay rate for lower values of $M_N \sim 100$ GeV. However, as M_N increases these branching ratios increase to retain a $\sim 25\%$ level. Both these channels can contribute to the

³ For Case-II, although BRs to different channels likely to change, we do not show the corresponding plot as final production cross-section for both the cases, after putting all the selection criteria, is very low for NH and beyond the reach of LHC at 14 TeV even with a luminosity of 3000 fb^{-1} .

⁴ Evidently former decay mode leads to opposite sign dileptons (OSDL), also suppressed by $|V_{lN}|^4$, but slightly larger compare to tri-lepton signal. However, significant irreducible backgrounds can come from $t\bar{t}$, VV (with $V = W, Z$), as well as $Z + Jets$ after vetoing dilepton invariant mass at Z -pole. Hence we are not considering the OSDL as a signal. Estimate of these backgrounds for OSDL can be found in [69]. Note that their more specific selection criteria are not applicable for our present signal. Similarly, OSDL through VBF is suppressed by $|V_{lN}|^4$ and is beset with large background coming from WW , $\tau\tau$ and ZZ production at VBF[57].

tri-lepton signal via leptonic decays and we have considered their contributions in our simulation. However since we will apply Z-veto (to minimize the SM background), the contribution coming from $Z\nu$ decay mode will be suppressed after final event selection.

As lepton Yukawa is small, the $H\nu$ mode is also not going to contribute to our signal even for higher values of M_N .

4. SIMULATION AND RESULTS

We have implemented the model in `FeynRules` [70] and generated the Feynman rules compatible with `MadGraph5` [71]. After generating Les Houches Event (LHE) [72] file from `MadGraph`, we have passed that to `PYTHIA6` [73] for showering and hadronization.

4.1. Selection criteria

To get enhancement in signal over background, we use the following selection criteria [74, 75]:

- ◊ Identification criteria of a lepton: pseudorapidity $|\eta_\ell| < 2.5$ and $p_{T\ell} > 20$ GeV have been used.
- ◊ Detector efficiency for leptons [76, 77]:
 - For electron (either e^- or e^+) detector efficiency is 0.7 (70%);
 - For muon (either μ^- or μ^+) detector efficiency is 0.9 (90%).
- ◊ Smearing⁵ of electron energy and muon p_T are incorporated.
- ◊ Lepton-lepton separation: for this $\Delta R_{ll} \geq 0.2$ is used⁶ (due to detector resolution of leptons).
- ◊ Lepton-photon separation: this is taken as $\Delta R_{l\gamma} \geq 0.2$ with all the photons having $p_{T\gamma} > 10$ GeV.
- ◊ Lepton-jet separation: The separation of a lepton with all the jets is set at $\Delta R_{lj} \geq 0.4$; otherwise that lepton is not counted as lepton. Jets are constructed from hadrons using `PYCELL` within the `PYTHIA`.

⁵ Choice of corresponding η dependent parameters is similar to one of our earlier work [74].

⁶ Here $\Delta R_{ij} = \sqrt{(\eta_i - \eta_j)^2 - (\phi_i - \phi_j)^2}$ quantifies the separation between particles i and j in the pseudorapidity(η)-azimuth(ϕ) plane.

- ◇ Hadronic activity cut: This cut is applied to take only pure kind of leptons that have very less hadronic activity around them. The hadronic activity within the cone of radius 0.2 around the lepton should be small, $\frac{\sum p_{T_{hadron}}}{p_{T_l}} \leq 0.2$.
- ◇ Hard p_T cuts used are: $p_{T_{l_1}} > 30$ GeV, $p_{T_{l_2}} > 30$ GeV and $p_{T_{l_3}} > 20$ GeV.
- ◇ Missing p_T cut: Due to the presence of neutrino, a missing p_T cut (> 30 GeV) is applied.
- ◇ Z-veto⁷ is applied to suppress the SM background.
- ◇ VBF cuts [55, 78]:
 - Central jet veto is also applied, in which we consider any jet with $E_{T3} > 20$ GeV and compute the rapidity with respect to the average of the two forward jets: $\eta_0 = \eta_3 - (\eta_1 + \eta_2)/2$. We veto the event if $|\eta_0| < 2$. Central jet veto is applied to suppress the QCD background substantially.
 - Charged leptons need to fall in between the rapidities of two forward tagging jets i.e. $\eta_{j,min} < \eta_\ell < \eta_{j,max}$.
 - p_T of jets: $p_{T_{j_1,j_2}} > 20$ GeV.
 - Invariant mass of jets: $M_{j_1j_2} > 600$ GeV.
 - Pseudorapidity of jets: $\eta_{j_1}, \eta_{j_2} < 0$ and $|\eta_{j_1} - \eta_{j_2}| > 4$. Demanding both the tagged jets in opposite hemisphere and a large rapidity separation among them significantly reduces the BG for VBF.

4.2. Background

4.2.1. For s -channel signal

To calculate the SM background we consider all channels that can produce or mimic the tri-lepton production with missing P_T . We closely follow the reference [74, 79] where similar background analysis was done with the event selection criteria listed as above except the cuts related to the VBF. Events are generated using ALPGEN [80] for the processes coming from $t\bar{t}$, $t\bar{t}(Z/\gamma^*)$, $t\bar{t}W^\pm$, $W^\pm(Z/\gamma^*)$, $(Z/\gamma^*)(Z/\gamma^*)$ at the parton level and passed into PYTHIA. As expected $t\bar{t}$ and

⁷ Same flavored but opposite sign lepton pair invariant mass $m_{\ell_1\ell_2}$ must be sufficiently away from Z mass, such that, typically, $|m_{\ell_1\ell_2} - M_Z| \geq 6\Gamma_Z \sim 15$ GeV.

Process	Cross section (<i>fb</i>)				
	$\ell\ell\ell$	eee	$ee\mu$	$e\mu\mu$	$\mu\mu\mu$
$t\bar{t}$	18.972	1.1383	7.0831	8.2214	2.5297
$W^\pm(Z/\gamma^*)$	10.832	0.0677	0.1311	5.9891	4.6440
$(Z/\gamma^*)(Z/\gamma^*)$	1.175	0.0734	0.0525	0.6400	0.4090
$t\bar{t}(Z/\gamma^*)$	1.103	0.0429	0.1329	0.4997	0.4275
$t\bar{t}W^\pm$	0.639	0.0328	0.2655	0.2424	0.0983
TOTAL	32.721	1.3551	7.6651	15.5926	8.1085

TABLE II: Dominant Standard Model background cross sections contributing to tri-lepton and missing transverse energy. These are calculated satisfying all the cuts (except VBF cuts) for the 14 TeV LHC. For each process we also classify the tri-lepton background into four different flavor combinations and present the cross section in each case along with the total contribution.

$W^\pm(Z/\gamma^*)$ contribute dominantly. These and other SM backgrounds are listed in Table II. For each process we classify the tri-lepton signals into four different flavor combinations and compute the cross section in each case along with the total contribution.

4.2.2. For VBF signal

Tri-lepton signal with missing P_T and two forward jets in VBF can be faked by different SM backgrounds. Processes like $t\bar{t}$ would produce b-jets and mostly effective in central region. Vetoing on jet activities in central region can eliminate most of the non-VBF type SM processes. However most important irreducible background comes from $W^\pm Z$ and ZZ together with two extra forward jets once the gauge bosons decay leptonically. These processes can construct dominant SM background for the VBF production of $3\ell + \cancel{E}_T$ since they includes the typical VBF topology and hence can easily pass the central jet veto criteria. These backgrounds are calculated⁸ using **MadGraph5** and **PYTHIA6**. In the Table III the dominant background cross sections after satisfying all the cuts including VBF cuts at 14 TeV LHC is tabulated. Like the case of s-channel backgrounds, for each process we also classify the tri-lepton signals into four different flavor combinations and compute the cross section in each case as well as the total contribution.

⁸ Next to leading order QCD corrections are available in [66, 67].

Process	Cross section (fb)				
	$\ell\ell\ell$	eee	$ee\mu$	$e\mu\mu$	$\mu\mu\mu$
W^+Zjj	0.04068	0.00073	0.00105	0.02157	0.01734
W^-Zjj	0.01923	0.00038	0.00055	0.00994	0.00836
$ZZjj$	0.00094	0.00002	0.00002	0.00066	0.00024
TOTAL	0.06085	0.00113	0.00162	0.03216	0.02594

TABLE III: Dominant Standard Model background cross section contributing to tri-lepton and missing transverse energy associated with two forward jets. These are calculated satisfying all the cuts including VBF cuts for the 14 TeV LHC. Cross sections of four different flavor combinations as well as the total cross section are listed.

4.3. Signal

Earlier in section. 3 we have presented the total heavy neutrino production cross sections for different light neutrino hierarchy with basic selection criteria. The cross section for NH scenario was found to be much lower than the IH scenario for s -channel. The branching ratios for decays of N to final states with μ and e are also very small for NH. Therefore we will concentrate only on IH scenario henceforth. For this we consider both s -channel and VBF process. Although the VBF cross-section for IH is lower or comparable to s -channel cross-section for NH for lower values of M_N , the background for VBF processes are much smaller. Hence we study this channel also for IH. In this section we consider all leptonic decay modes of heavy neutrinos for a benchmark mass of M_N at 100 GeV with the cuts discussed in section. 4.1.

4.3.1. Signal for s -channel

The signal coming from decay of heavy neutrinos

$$pp \rightarrow \ell^\pm N \rightarrow \ell^\pm (\ell^\mp W^\pm) \rightarrow \ell^\pm \ell^\mp \ell^\pm + \cancel{E}_T, \quad \text{where } \ell \equiv e, \mu.$$

Table IV lists the final tri-lepton signal cross section through s -channel heavy neutrino production at 14 TeV LHC for the benchmark point $M_N = 100$ GeV incorporating all event selection criteria except VBF cuts as described earlier. The total contribution from the light leptons as well as the contributions from the four different flavor combinations are presented.

As we can see from the Table IV cross section in terms of flavors has the ordering: $ee\mu > eee > e\mu\mu > \mu\mu\mu$. We can understand this in the following way. There are total 8 possibilities which

Hierarchy	Cross section (<i>fb</i>)				
	$\ell\ell\ell$	eee	$ee\mu$	$e\mu\mu$	$\mu\mu\mu$
IH	27.07	10.297	16.314	0.459	0.0

TABLE IV: Cross section for IH case. Final tri-lepton signal cross section through s-channel heavy neutrino production at the 14 TeV LHC for the benchmark point $M_N = 100$ GeV including all event selection cuts except VBF cuts. We classify the tri-lepton signals into four different flavor combinations and present the cross section in each case along with the total light lepton contribution.

can produce $\ell\ell\ell$ events. There is only one way to produce $\mu\mu\mu$ and eee final states. However, there are three possible ways to get the $ee\mu$ channel depending on which one of ℓ_i 's in figure 2 is associated with e and μ . Similarly for the $e\mu\mu$ final state also we get 3 possibilities. The amplitude for eee channel $\sim V_{eN}^4$; the $ee\mu$ channel goes as $\sim V_{eN}^2 + 2V_{eN}V_{\mu N}$; the $e\mu\mu$ channel goes as $\sim V_{\mu N}^2 + 2V_{eN}V_{\mu N}$ while the $\mu\mu\mu$ channel as $\sim V_{\mu N}^2$. Since $V_{eN} \gg V_{\mu N}$, the eee and $ee\mu$ cross sections are much larger whereas $\mu\mu\mu$ cross section is negligible. $ee\mu$ cross section is higher than the eee cross section because of higher muon efficiency in the detector, whereas the small $e\mu\mu$ cross section is due to a very tiny value of $V_{\mu N}$.

One can also compute the ratios of events with different flavour compositions in which some of the common systematic uncertainties can get cancelled. For example $ee\mu/eee \sim \epsilon$ where ϵ denotes the relative efficiency of detection of muon over electron, $ee\mu/\mu\mu\mu \sim \epsilon V_{eN}^4/V_{\mu N}^4$; $eee/e\mu\mu \sim \epsilon^2 V_{eN}^4/V_{\mu N}^4$ etc. Since for a fixed y_ν , which in turn implies specific values for phases, the variation of the light-heavy mixing angles are not very much with oscillation parameters, these ratios vary within a very narrow range⁹ and hence can be used to test the model. Ofcourse for different phase choices a different y_ν and hence different predictions can be obtained. However, a smaller value in y_ν would result in a lower event rate and hence it would be difficult to test at the LHC.

4.3.2. Signal for VBF

In this section we present the results for the case where N is produced by VBF:

$$pp \rightarrow \ell^\pm N jj \rightarrow \ell^\pm (\ell^\mp W^\pm) jj \rightarrow \ell^\pm \ell^\mp \ell^\pm + \cancel{E}_T + jj(\text{forward jets}), \quad \text{where } \ell \equiv e, \mu.$$

⁹ Note that, the allowed magnitude of mixings are as following: For a fixed value of $y_\nu (= 0.4)$, $\alpha (= 3\pi/4)$, $\delta (= 0)$ and $M_N (= 100)$ GeV, the magnitude of $|V_{eN}|$ and $|V_{\mu N}|$ vary in a very small range for 3σ variation of oscillation parameters; $|V_{eN}| = 0.471 - 0.484$, $|V_{\mu N}| = 1.236 \times 10^{-4} - 1.272 \times 10^{-4}$. However, $|V_{\tau N}|$ varies little higher; $|V_{\tau N}| = 0.092 - 0.147$. Since we are considering modes involving only e and μ , the cross sections are likely to vary by a small amount for different set of oscillation parameters.

Hierarchy	Cross section (fb)				
	$\ell\ell\ell$	eee	$ee\mu$	$e\mu\mu$	$\mu\mu\mu$
IH	0.018068	7.09×10^{-3}	1.06×10^{-2}	4.06×10^{-4}	0.00

TABLE V: Final tri-lepton Signal through VBF production of heavy neutrino for the benchmark point $M_N = 100$ GeV at 14 TeV LHC for IH after all event selection cuts.

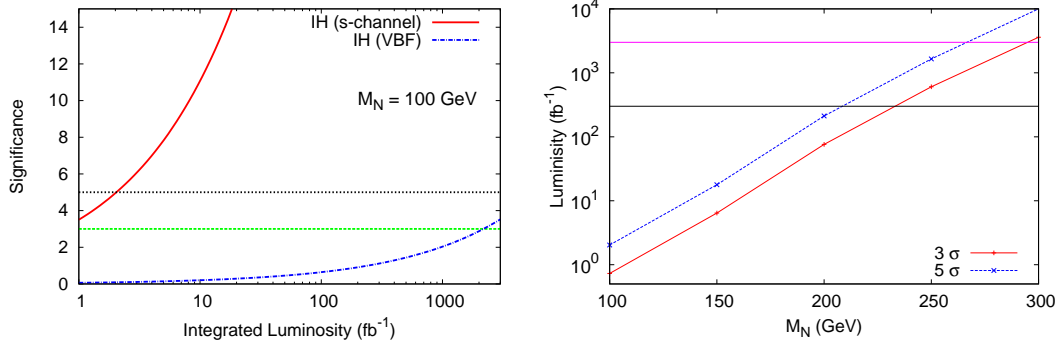


FIG. 6: (Left) The variation of significance $S/\sqrt{S+B}$ for the s-channel production signal for benchmark point $M_N = 100$ GeV with the integrated luminosity available for the low luminosity option at 14 TeV LHC. Black-dotted (green-dashed) line parallel to the x-axis represents 5 σ (3 σ) significance. (Right) The lines for 3 σ (red) and 5 σ (blue) significance in terms of heavy neutrino mass and integrated luminosity. With 300 fb^{-1} luminosity at LHC14 the heavy neutrino mass in this model can be probed up to $\sim 210(230)$ GeV with $\sim 5\sigma$ (3 σ) significance. For very high luminosity of 3000 fb^{-1} this can reach up to $\sim 270(295)$ GeV.

In Table V we present the final tri-lepton signal cross sections through VBF production of heavy neutrinos at the 14 TeV LHC for the benchmark point $M_N = 100$ GeV, after including all cuts. Here we have only shown the case of inverted hierarchy and signal is found to be quite small. Although VBF backgrounds are small, the tiny production cross sections are insufficient for giving any signal with integrated luminosity of 300 fb^{-1} . Some indications from VBF can appear only at the HL-LHC (3000 fb^{-1}). However, 5 σ significance can not be reached even for $M_N = 100$ GeV.

5. DISCOVERY POTENTIAL

After numerical computation of all necessary signals and backgrounds, results are better represented in terms of significance, defined as $S/\sqrt{S+B}$, where $S(B) = \mathcal{L}\sigma_{S(B)}$. Here \mathcal{L} being integrated luminosity available for the collider at certain machine energy and $\sigma_{S(B)}$ is the final cross section after all event selection, for given parameters like heavy neutrino mass and corresponding allowed couplings. Fig. 6 (Left) demonstrates the expected significance coming from

s-channel production of heavy Dirac neutrino of mass 100 GeV as a function of integrated luminosity at 14 TeV LHC. In the figure black-dotted (green-dashed) line shows 5σ (3σ) significance. From the figure it is clear that for the case of s-channel signal in the IH scenario, $3\sigma(5\sigma)$ significance can be achieved within the integrated luminosity $\sim 0.73(2.03) \text{ fb}^{-1}$. In the case of VBF channel 3σ significance can be achieved with 2175 fb^{-1} luminosity, while 5σ significance is not achievable within 3000 fb^{-1} luminosity which is planned for the HL-LHC.

Fig. 6 (Right) shows the lines for 3σ (red) and 5σ (blue) significance in terms of heavy neutrino mass and integrated luminosity. With 300 fb^{-1} luminosity at LHC14 the heavy neutrino mass in this model can be probed up to $\sim 210(230) \text{ GeV}$ with $\sim 5\sigma$ (3σ) significance. For very high luminosity of 3000 fb^{-1} this can reach up to $\sim 270(295) \text{ GeV}$. For VBF signal, since $M_N = 100 \text{ GeV}$ itself requires a very large integrated luminosity; higher values of M_N are not possible to explore.

6. SUMMARY AND CONCLUSION

In this work we have considered TeV scale minimal linear seesaw model which generates correct order of light neutrino masses and has sizable light-heavy mixing to produce heavy neutrinos at colliders like LHC. One of the important features of this model is that it can be fully reconstructible from oscillation data excepting an overall factor y_ν characterizing the Dirac Yukawa matrix. However this parameter gets constrained by LFV and vacuum meta-stability bounds. The neutral fermion mass spectrum of this model consists of one massless, two light and two heavy neutrinos.

We have studied the collider phenomenology of TeV scale linear seesaw at 14 TeV LHC. The heavy neutrinos in this model can be dominantly produced through the s-channel. In a leading order calculation, subsequent decay of these leads to characteristic tri-lepton signal with missing p_T . We also consider the production of heavy neutrinos through the VBF process. The signal for this is tri-leptons with additional two forward jets which can be tagged. Both these signals as well as SM backgrounds have been estimated with realistic simulations using **MadGraph** and **PYTHIA**.

We found that s-channel tri-lepton production process have potential to be discovered at the LHC for IH scenario. However due to severe constraint on the light-heavy mixing coming from LFV in the case of NH scenario, both s-channel and VBF can not be probed at the 14 TeV LHC with proposed luminosity. For a benchmark point with a heavy neutrino mass $M_N = 100 \text{ GeV}$, 3σ significance can be achieved with integrated luminosity of $\sim 0.73(2175) \text{ fb}^{-1}$ for s-channel(VBF) signal in the IH scenario. 5σ significance can be reached for s-channel signal with a integrated

luminosity of $\sim 2 \text{ fb}^{-1}$, however for VBF signal the required luminosity is $\sim 6042 \text{ fb}^{-1}$, which is beyond the reach of projected luminosity at the LHC. Discovery reach in the tri-lepton channel can be achieved upto the heavy neutrino mass of $\sim 210(230) \text{ GeV}$ with $\sim 5\sigma$ (3σ) significance at the low luminosity (300 fb^{-1}) option of 14 TeV LHC. In the high luminosity (3000 fb^{-1}) search, reach is upto $\sim 270(295) \text{ GeV}$. Whereas, VBF channel can only reach upto $\sim 3\sigma$ for M_N at 100 GeV. Our analysis uses values for the elements, V_{lN} of the light-heavy mixing matrix, which are consistent with the constraints coming from vacuum metastability and LFV. Any freedom of choosing larger values (e.g. $\sim \mathcal{O}(1)$) for these parameters can extend the discovery limit by a very significant amount. With the constraints used in this work, for V_{lN} , a detectable tri-lepton signal can only be obtained for the inverted hierarchical scenario with particular choices of phases leading to large y_ν . One can also compute the ratios of events with different flavour compositions which are proportional to the elements V_{lN} . They vary only within a narrow range with the 3σ variations of oscillation parameters and thus the model has very definite predictions for these ratios.

-
- [1] G. Aad et al. (ATLAS Collaboration), Phys.Lett. **B716**, 1 (2012), arXiv:1207.7214 [hep-ex]
 - [2] S. Chatrchyan et al. (CMS Collaboration), Phys.Lett. **B716**, 30 (2012), arXiv:1207.7235 [hep-ex]
 - [3] P. Ade et al. (Planck Collaboration)(2013), arXiv:1303.5076 [astro-ph.CO]
 - [4] S. Weinberg, Phys.Rev.Lett. **43**, 1566 (1979)
 - [5] P. Minkowski, Phys.Lett. **B67**, 421 (1977)
 - [6] T. Yanagida, Conf.Proc. **C7902131**, 95 (1979)
 - [7] M. Gell-Mann, P. Ramond, and R. Slansky, Conf.Proc. **C790927**, 315 (1979)
 - [8] S. Glashow, NATO Adv.Study Inst.Ser.B Phys. **59**, 687 (1980)
 - [9] R. N. Mohapatra and G. Senjanovic, Phys.Rev.Lett. **44**, 912 (1980)
 - [10] A. Pilaftsis, Z.Phys. **C55**, 275 (1992), arXiv:hep-ph/9901206 [hep-ph]
 - [11] J. Gluza, Acta Phys.Polon. **B33**, 1735 (2002), arXiv:hep-ph/0201002 [hep-ph]
 - [12] A. Pilaftsis, Phys.Rev.Lett. **95**, 081602 (2005), arXiv:hep-ph/0408103 [hep-ph]
 - [13] J. Kersten and A. Y. Smirnov, Phys.Rev. **D76**, 073005 (2007), arXiv:0705.3221 [hep-ph]
 - [14] Z.-z. Xing, Prog.Theor.Phys.Suppl. **180**, 112 (2009), arXiv:0905.3903 [hep-ph]
 - [15] X.-G. He, S. Oh, J. Tandean, and C.-C. Wen, Phys.Rev. **D80**, 073012 (2009), arXiv:0907.1607 [hep-ph]
 - [16] A. Ibarra, E. Molinaro, and S. Petcov, JHEP **1009**, 108 (2010), arXiv:1007.2378 [hep-ph]
 - [17] F. F. Deppisch and A. Pilaftsis, Phys.Rev. **D83**, 076007 (2011), arXiv:1012.1834 [hep-ph]
 - [18] R. Adhikari and A. Raychaudhuri, Phys.Rev. **D84**, 033002 (2011), arXiv:1004.5111 [hep-ph]
 - [19] I. Gogoladze, N. Okada, and Q. Shafi, Phys.Lett. **B672**, 235 (2009), arXiv:0809.0703 [hep-ph]
 - [20] K. Babu, S. Nandi, and Z. Tavartkiladze, Phys.Rev. **D80**, 071702 (2009), arXiv:0905.2710 [hep-ph]

- [21] F. Bonnet, D. Hernandez, T. Ota, and W. Winter, JHEP **0910**, 076 (2009), arXiv:0907.3143 [hep-ph]
- [22] S. Kanemura and T. Ota, Phys.Lett. **B694**, 233 (2010), arXiv:1009.3845 [hep-ph]
- [23] Y. Liao, G.-Z. Ning, and L. Ren, Phys.Rev. **D82**, 113003 (2010), arXiv:1008.0117 [hep-ph]
- [24] I. Picek and B. Radovic, Phys.Lett. **B687**, 338 (2010), arXiv:0911.1374 [hep-ph]
- [25] Y. Liao, JHEP **1106**, 098 (2011), arXiv:1011.3633 [hep-ph]
- [26] K. Kumericki, I. Picek, and B. Radovic, Phys.Rev. **D86**, 013006 (2012), arXiv:1204.6599 [hep-ph]
- [27] K. L. McDonald, JHEP **1307**, 020 (2013), arXiv:1303.4573 [hep-ph]
- [28] A. Zee, Phys.Lett. **B93**, 389 (1980)
- [29] A. Zee, Nucl.Phys. **B264**, 99 (1986)
- [30] K. Babu, Phys.Lett. **B203**, 132 (1988)
- [31] L. M. Krauss, S. Nasri, and M. Trodden, Phys.Rev. **D67**, 085002 (2003), arXiv:hep-ph/0210389 [hep-ph]
- [32] E. Ma, Phys.Rev. **D73**, 077301 (2006), arXiv:hep-ph/0601225 [hep-ph]
- [33] M. Aoki, S. Kanemura, and O. Seto, Phys.Rev.Lett. **102**, 051805 (2009), arXiv:0807.0361 [hep-ph]
- [34] P. B. Dev and A. Pilaftsis, Phys.Rev. **D86**, 113001 (2012), arXiv:1209.4051 [hep-ph]
- [35] M. Gustafsson, J. M. No, and M. A. Rivera(2014), arXiv:1402.0515 [hep-ph]
- [36] R. Mohapatra and J. Valle, Phys.Rev. **D34**, 1642 (1986)
- [37] W.-Y. Keung and G. Senjanovic, Phys.Rev.Lett. **50**, 1427 (1983)
- [38] A. Datta, M. Guchait, and A. Pilaftsis, Phys.Rev. **D50**, 3195 (1994), arXiv:hep-ph/9311257 [hep-ph]
- [39] T. Han and B. Zhang, Phys.Rev.Lett. **97**, 171804 (2006), arXiv:hep-ph/0604064 [hep-ph]
- [40] S. Bray, J. S. Lee, and A. Pilaftsis, Nucl.Phys. **B786**, 95 (2007), arXiv:hep-ph/0702294 [HEP-PH]
- [41] F. del Aguila, J. Aguilar-Saavedra, and R. Pittau, JHEP **0710**, 047 (2007), arXiv:hep-ph/0703261 [hep-ph]
- [42] F. del Aguila and J. Aguilar-Saavedra, Nucl.Phys. **B813**, 22 (2009), arXiv:0808.2468 [hep-ph]
- [43] A. Atre, T. Han, S. Pascoli, and B. Zhang, JHEP **0905**, 030 (2009), arXiv:0901.3589 [hep-ph]
- [44] S. Chatrchyan et al. (CMS Collaboration), Phys.Lett. **B717**, 109 (2012), arXiv:1207.6079 [hep-ex]
- [45] P. S. B. Dev, A. Pilaftsis, and U.-k. Yang, Phys.Rev.Lett. **112**, 081801 (2014), arXiv:1308.2209 [hep-ph]
- [46] A. Das, P. Bhupal Dev, and N. Okada(2014), arXiv:1405.0177 [hep-ph]
- [47] F. del Aguila and J. Aguilar-Saavedra, Phys.Lett. **B672**, 158
- [48] C.-Y. Chen and P. B. Dev, Phys.Rev. **D85**, 093018 (2012), arXiv:1112.6419 [hep-ph]
- [49] A. Das and N. Okada(2012), arXiv:1207.3734 [hep-ph]
- [50] O. Eboli, J. Gonzalez-Fraile, and M. Gonzalez-Garcia, JHEP **1112**, 009 (2011), arXiv:1108.0661 [hep-ph]
- [51] S. Chatrchyan et al. (CMS Collaboration)(2014), arXiv:1404.5801 [hep-ex]
- [52] M. Gavela, T. Hambye, D. Hernandez, and P. Hernandez, JHEP **0909**, 038 (2009), arXiv:0906.1461 [hep-ph]
- [53] S. Khan, S. Goswami, and S. Roy, Phys.Rev. **D89**, 073021 (2014), arXiv:1212.3694 [hep-ph]
- [54] M. Malinsky, T. Ohlsson, Z.-z. Xing, and H. Zhang, Phys.Lett. **B679**, 242 (2009),

- arXiv:0905.2889 [hep-ph]
- [55] D. L. Rainwater(1999), arXiv:hep-ph/9908378 [hep-ph]
 - [56] A. Datta, P. Konar, and B. Mukhopadhyaya, Phys.Rev.Lett. **88**, 181802 (2002), arXiv:hep-ph/0111012 [hep-ph]
 - [57] D. Choudhury, A. Datta, K. Huitu, P. Konar, S. Moretti, et al., Phys.Rev. **D68**, 075007 (2003), arXiv:hep-ph/0304192 [hep-ph]
 - [58] G.-C. Cho, K. Hagiwara, J. Kanzaki, T. Plehn, D. Rainwater, et al., Phys.Rev. **D73**, 054002 (2006), arXiv:hep-ph/0601063 [hep-ph]
 - [59] P.-H. Gu and U. Sarkar, Phys.Lett. **B694**, 226 (2010), arXiv:1007.2323 [hep-ph]
 - [60] H. Zhang and S. Zhou, Phys.Lett. **B685**, 297 (2010), arXiv:0912.2661 [hep-ph]
 - [61] M. Hirsch, S. Morisi, and J. Valle, Phys.Lett. **B679**, 454 (2009), arXiv:0905.3056 [hep-ph]
 - [62] F. Bazzocchi, Phys.Rev. **D83**, 093009 (2011), arXiv:1011.6299 [hep-ph]
 - [63] W. Grimus and L. Lavoura, JHEP **0011**, 042 (2000), arXiv:hep-ph/0008179 [hep-ph]
 - [64] S. Khan, Nucl.Phys. **B864**, 38 (2012), arXiv:1203.5043 [hep-ph]
 - [65] J. de Blas, EPJ Web Conf. **60**, 19008 (2013), arXiv:1307.6173 [hep-ph]
 - [66] G. Bozzi, B. Jager, C. Oleari, and D. Zeppenfeld, Phys.Rev. **D75**, 073004 (2007), arXiv:hep-ph/0701105 [hep-ph]
 - [67] B. Jager, C. Oleari, and D. Zeppenfeld, Phys.Rev. **D73**, 113006 (2006), arXiv:hep-ph/0604200 [hep-ph]
 - [68] J. Pumplin, D. Stump, J. Huston, H. Lai, P. M. Nadolsky, et al., JHEP **0207**, 012 (2002), arXiv:hep-ph/0201195 [hep-ph]
 - [69] J. Eckel, M. J. Ramsey-Musolf, W. Shepherd, and S. Su, JHEP **1411**, 117 (2014), arXiv:1408.2841 [hep-ph]
 - [70] N. D. Christensen and C. Duhr, Comput.Phys.Commun. **180**, 1614 (2009), arXiv:0806.4194 [hep-ph]
 - [71] J. Alwall, M. Herquet, F. Maltoni, O. Mattelaer, and T. Stelzer, JHEP **1106**, 128 (2011), arXiv:1106.0522 [hep-ph]
 - [72] J. Alwall, A. Ballestrero, P. Bartalini, S. Belov, E. Boos, et al., Comput.Phys.Commun. **176**, 300 (2007), arXiv:hep-ph/0609017 [hep-ph]
 - [73] T. Sjostrand, S. Mrenna, and P. Z. Skands, JHEP **0605**, 026 (2006), arXiv:hep-ph/0603175 [hep-ph]
 - [74] G. Bambhaniya, J. Chakraborty, S. Goswami, and P. Konar, Phys.Rev. **D88**, 075006 (2013), arXiv:1305.2795 [hep-ph]
 - [75] B. Mukhopadhyaya and S. Mukhopadhyay, Phys.Rev. **D82**, 031501 (2010), arXiv:1005.3051 [hep-ph]
 - [76] G. Aad et al. (ATLAS Collaboration)(2009), arXiv:0901.0512 [hep-ex]
 - [77] G. Bayatian et al. (CMS Collaboration), J.Phys. **G34**, 995 (2007)
 - [78] E. Yazgan, J. Damgov, N. Akchurin, V. Genchev, D. Green, et al., Eur.Phys.J. **C53**, 329 (2008), arXiv:0706.1898 [hep-ex]
 - [79] G. Bambhaniya, J. Chakraborty, J. Gluza, M. Kordiaczynska, and R. Szafron, JHEP **1405**, 033 (2014), arXiv:1311.4144 [hep-ph]

- [80] M. L. Mangano, M. Moretti, F. Piccinini, R. Pittau, and A. D. Polosa, JHEP **0307**, 001 (2003), arXiv:hep-ph/0206293 [hep-ph]